Journal of Low Temperature Physics, Vol. 133, Nos. 5/6, December 2003 (© 2003)

Separable Model Calculations for the Anisotropic Properties of MgB_2

M. Zehetmayer,[1] H. W. Weber,[1] and E. Schachinger[2]

[1] *Atomic Institute of the Austrian Universities, A-1020 Vienna, Austria*
E-mail: zehetm@ati.ac.at
[2] *Institut für Theoretische Physik, Technische Universität Graz, A-8010 Graz, Austria*

(Received June 10, 2003; revised August 8, 2003)

The Migdal–Eliashberg equations are solved using the separable model for the electron-phonon coupling and the Fermi velocity. We show that this very simple model is capable of describing particular properties of superconducting MgB_2 and is, therefore, very convenient to discuss the specific effects of anisotropy. The temperature dependence of the specific heat, the upper and the thermodynamic critical field is calculated and found to be in excellent agreement with experimental results for a certain set of model parameters.

KEY WORDS: Migdal–Eliashberg equations; separable model; anisotropy.

1. INTRODUCTION

A large number of publications on experimental and theoretical results clarified many aspects of the new superconductor MgB_2.[1] There is almost no doubt, that superconductivity is mediated by electron-phonon (e^--ph) coupling and that *s*-wave pairing prevails. The Fermi surface of MgB_2 was calculated by several groups and found to be not very complicated, but strongly anisotropic.[2–4] The anisotropy of macroscopic superconducting properties, such as the upper critical field, was soon confirmed by experiments on single crystals.[5–7] For a theoretical analysis, the fully anisotropic Eliashberg (Eb) equations have to be solved using the complete **k** (wavevector) dependent e^--ph coupling matrix and the Coulomb pseudopotentials. Very often, not only the calculations, but also the interpretation of the results become difficult, especially if the relevant physical mechanism responsible for a particular feature is to be clarified.

0022-2291/03/1200-0407/0 © 2003 Plenum Publishing Corporation

Several models are available, which simplify the Eb equations, but still take anisotropy effects into account. The two (or N) band and the separable model are among them. The latter is particularly simple as it introduces only two anisotropy parameters, one for the e^--ph coupling strength ($\langle a_{\mathbf{k}}^2 \rangle$) and one for the anisotropy of the Fermi velocity ($\langle b_{\mathbf{k}}^2 \rangle$). Simple models often allow to concentrate on features which dominate a phenomenon and for a superconductor it is of quite some importance to know which phonon modes dominate. It was demonstrated by Manalo and Schachinger[8] for borocarbides that single or double peak e^--ph interaction spectral densities $\alpha^2F(\omega)$ could be constructed, which together with appropriately chosen parameters $\langle a_{\mathbf{k}}^2 \rangle$ and $\langle b_{\mathbf{k}}^2 \rangle$ allowed a good reproduction of experimental data on the temperature dependence of the thermodynamics and of the upper critical field, $H_{c2}(T)$. The phonon modes which correspond to the delta peaks in the $\alpha^2F(\omega)$ spectrum can then be interpreted as being most important to superconductivity.

The Fermi surface of MgB_2 shows four Fermi surface sheets[9–11] (two σ-bands and two π-bands) and the gap has two sharp maxima, $\Delta_\pi \approx 1.7$ meV and $\Delta_\sigma \approx 7$ meV. Kogan[12] pointed out, focusing on the macroscopic superconducting anisotropy γ within Ginzburg–Landau theory, that a model with two gaps and two sheets of the Fermi surface may prove useful in relating the various macroscopic properties of MgB_2. In Eliashberg theory this is easily accomplished within the separable model ansatz. This ansatz is shortly reviewed in Sec. 2. Section 3 applies the separable model to MgB_2 using an Einstein spectrum for $\alpha^2F(\omega)$ and the anisotropy parameters $\langle a_{\mathbf{k}}^2 \rangle$ and $\langle b_{\mathbf{k}}^2 \rangle$ to fit theoretical results to experimental data for the specific heat difference $\Delta C(T)$ and for the upper critical field $H_{c2}(T)$. The results of this procedure are discussed in detail as is the relevance of these model calculations. Finally, in Sec. 4, we present our conclusions.

2. THEORY

The separable model was originally introduced into BCS theory[13] and later adapted for the Eb theory.[14,15] Within this model, the anisotropic e^--ph interaction spectral function is described by[14]

$$\alpha^2F(\omega)_{\mathbf{k},\mathbf{k}'} = (1+a_{\mathbf{k}})\,\alpha^2F(\omega)(1+a_{\mathbf{k}'}), \tag{1}$$

with $\mathbf{k}$ and $\mathbf{k}'$ the incoming and outgoing quasiparticle momentum vectors in the e^--ph scattering process, $a_{\mathbf{k}}$ an anisotropy function with the important feature that its Fermi surface average $\langle a_{\mathbf{k}} \rangle = 0$, and $\alpha^2F(\omega)$ the e^--ph

interaction spectral density of the equivalent isotropic system. A similar ansatz is applied to describe the anisotropy of the Fermi velocity[15]

$$v_{F,\mathbf{k}} = (1+b_{\mathbf{k}})\langle v_{\mathrm{F}}\rangle. \tag{2}$$

Here, $\langle v_{\mathrm{F}}\rangle$ is the Fermi surface average of the Fermi velocity and $b_{\mathbf{k}}$ is an anisotropy function defined in the same way as $a_{\mathbf{k}}$. In principle, the separable model assumes anisotropy effects to be rather small and it is, thus, deemed to be sufficient to keep the mean square anisotropies $\langle a_{\mathbf{k}}^2\rangle$ and $\langle b_{\mathbf{k}}^2\rangle$ as the important anisotropy parameters.

The Eb equations, in the imaginary axis notation, for the renormalized quasiparticle frequencies $\tilde{\omega}_{\mathbf{k}}(n)$ and the Matsubara gaps $\tilde{\Delta}_{\mathbf{k}}(n)$ of an anisotropic superconductor in the clean limit are given by[16]

$$\tilde{\omega}_{\mathbf{k}}(n) = \omega_n + \pi T \sum_m \langle \lambda_{\mathbf{k},\mathbf{k}'}(m-n)\, f_{\mathbf{k}'}(m)\rangle' \tag{3}$$

$$\tilde{\Delta}_{\mathbf{k}}(n) = \pi T \sum_{|m|\leqslant c} \langle [\lambda_{\mathbf{k},\mathbf{k}'}(m-n) - \mu^*_{\mathbf{k},\mathbf{k}'}]\, g_{\mathbf{k}'}(m)\rangle', \tag{4}$$

with

$$f_{\mathbf{k}}(n) = \tilde{\omega}_{\mathbf{k}}(n)/\sqrt{\tilde{\Delta}_{\mathbf{k}}^2(n)+\tilde{\omega}_{\mathbf{k}}^2(n)} \tag{5}$$

$$g_{\mathbf{k}}(n) = \tilde{\Delta}_{\mathbf{k}}(n)/\sqrt{\tilde{\Delta}_{\mathbf{k}}^2(n)+\tilde{\omega}_{\mathbf{k}}^2(n)} \tag{6}$$

$$\lambda_{\mathbf{k},\mathbf{k}'}(m-n) = 2\int_0^\infty d\Omega\, \frac{\Omega\alpha^2 F(\Omega)_{\mathbf{k},\mathbf{k}'}}{\Omega^2+(\omega_m-\omega_n)^2}. \tag{7}$$

Here, $\omega_n = \pi T(2n+1)$, $n = 0, \pm 1, \pm 2, \ldots$ are the Matsubara frequencies, $\mu^*_{\mathbf{k},\mathbf{k}'}$ denotes the (anisotropic) Coulomb pseudopotential, c is a cutoff index related to the cutoff frequency ω_c, $\langle\cdots\rangle$ denotes the Fermi surface average, and, finally, T is the temperature.

Thermodynamics are calculated from the free energy difference between the normal and superconducting state which is given by[17]

$$\Delta F = N(0)\,\pi T \sum_{|n|\leqslant c} \langle [h_{\mathbf{k}}(n) - |\tilde{\omega}_{\mathbf{k}}(n)|][1-|\tilde{\omega}^0_{\mathbf{k}}(n)|/h_{\mathbf{k}}(n)]\rangle, \tag{8}$$

with

$$h_{\mathbf{k}}(n) = \sqrt{\tilde{\Delta}_{\mathbf{k}}^2(n)+\tilde{\omega}_{\mathbf{k}}^2(n)}. \tag{9}$$

Here, $N(0)$ denotes the total electronic density of states at the Fermi energy and $\tilde{\omega}_{\mathbf{k}}^{0}(n)$ are the renormalized normal-state quasiparticle frequencies which can be determined from Eq. (3) by setting $\tilde{\Delta}_{\mathbf{k}}(n) = 0$, which gives $f_{\mathbf{k}}(n) = \mathrm{sgn}(\omega_n)$. Using $\Delta F(T)$ we can calculate the thermodynamic critical field $H_c(T)$ and the specific heat difference between the normal and the superconducting state $\Delta C(T)$ using the relations

$$H_c(T) = \sqrt{2\Delta F/\mu_0} \tag{10}$$

$$\Delta C(T) = -T\,\partial^2 \Delta F(T)/\partial T^2. \tag{11}$$

μ_0 is the vacuum permeability.

At the transition temperature T_c the Matsubara gaps become infinitesimally small and, thus, $\tilde{\Delta}_{\mathbf{k}}^2(n)$ can be neglected giving $f_{\mathbf{k}}(n) = \mathrm{sgn}(\omega_n)$ and $g_{\mathbf{k}}(n) = \tilde{\Delta}_{\mathbf{k}}(n)/|\tilde{\omega}_{\mathbf{k}}(n)|$. This results in the so-called linearized Eb equations. At the upper critical field $H_{c2}(T)$ the superconductor undergoes a second order phase transition and, thus, determining $H_{c2}(T)$ is equivalent to the calculation of the critical temperature $T_c(H)$, for an applied magnetic field of strength H. Only $f_{\mathbf{k}}(n)$ and $g_{\mathbf{k}}(n)$ are to be modified[15]

$$f_{\mathbf{k}}(n) = \mathrm{sgn}(\omega_n) \tag{12}$$

$$g_{\mathbf{k}}(n) = \tilde{\Delta}_{\mathbf{k}}(n)\,\chi_{\mathbf{k}}(n) \tag{13}$$

$$\chi_{\mathbf{k}}(n) = \frac{2}{\sqrt{\beta_{\mathbf{k}}}} \int_0^\infty dx\, e^{-x^2} \tan^{-1}\left(\frac{x\sqrt{\beta_{\mathbf{k}}}}{|\tilde{\omega}_{\mathbf{k}}(n)|}\right) \tag{14}$$

$$\beta_{\mathbf{k}} = 0.5 q_e \mu_0 H_{c2}(T) \langle v_{\mathrm{F}} \rangle^2 (1 + b_{\mathbf{k}})^2, \tag{15}$$

for a given temperature T, where q_e is the charge of the electron.

In the simplest case, the Fermi surface is divided into two sheets ($s1$, $s2$), on which $a_{\mathbf{k}}$ and $b_{\mathbf{k}}$ are constant, i.e., they become a_{si} and b_{si} on sheet i. Furthermore, if we allow different electronic densities of states on each sheet with relative weights p_i ($p_1 + p_2 = 1$), then we find ($i, j = 1, 2$ or 2, 1):[18]

$$a_{si} = (-1)^{i-1} \sqrt{\langle a_{\mathbf{k}}^2 \rangle\, p_j/p_i} \tag{16}$$

$$b_{si} = (-1)^{i} \sqrt{\langle b_{\mathbf{k}}^2 \rangle\, p_j/p_i}\,. \tag{17}$$

3. RESULTS AND DISCUSSION

To evaluate the Eb equations, the spectral function $\alpha^2 F(\Omega)$ of MgB_2 is needed; it was calculated by several groups using ab-initio methods.[9, 10, 19, 20]

We employ a very simple Eb function with one peak at 76 meV (cf. Ref. 10) and with a width of 1 meV. The height is determined by the mass enhancement factor $\lambda = \lambda(0) = 2\int_0^\infty d\Omega\, \alpha^2 F(\Omega)/\Omega = 0.61$. This value is found experimentally in specific heat measurements[21, 22] and was confirmed theoretically.[10] To make our model complete, we set the maximum phonon (Debye) frequency ω_0 to 100 meV and choose $p_1 = p_2 = 0.5$. In our calculations $\omega_c = 6\omega_0$.

3.1. Transition Temperature

We start the calculations by solving the Eb equations for T_c in zero field, or actually, we set T_c to 38 K, a typical value for single crystals,[6] and calculate the appropriate Coulomb pseudopotential μ^*, that is assumed to be constant over the Fermi surface. Unfortunately, μ^* cannot be determined exactly from independent measurements or calculations, but is known to be approximately 0.1–0.2 in almost all superconductors.[24] For the isotropic case, we set $\langle a_k^2 \rangle = 0.0$ and obtain $\mu^* \simeq 0.045$, which is obviously very low. Turning on the anisotropy by increasing $\langle a_k^2 \rangle$ successively to 0.1, 0.2, and 0.3 changes μ^* to 0.072, 0.109, and 0.164. The latter two values are quite reasonable, and it will turn out in the following paragraphs that $\langle a_k^2 \rangle = 0.3$ is most suitable for reproducing the experimental data of MgB_2. Thus we fix $\mu^* = 0.164$ to investigate the influence of anisotropy on T_c. The corresponding isotropic T_c is found to be 16 K, which is considerably smaller than the experimental value and illustrates the huge influence of anisotropy on this quantity. For the intermediate anisotropy parameters $\langle a_k^2 \rangle = 0.1$, 0.2, we calculate $T_c = 23$ K and 30 K.

3.2. Specific Heat

The temperature dependence of $\Delta C(T)/(\gamma_n T)$ (Sommerfeld constant: $\gamma_n = 2/3\pi^2 k_B^2 N(0)[1+\lambda]$) only depends on the anisotropy parameter and is, therefore, convenient to determine $\langle a_k^2 \rangle$ by comparing theory with experiment. This is done in Fig. 1a for different anisotropies (but with T_c fixed at 38 K). A special quantity is the jump of the specific heat at T_c, $\Delta C(T_c)/(\gamma_n T_c)$. Its "universal" value in weak coupling isotropic (BCS) superconductors is 1.43, but generally increases with stronger coupling[24] (e.g., to 2.8 for Pb with $\lambda = 1.55$). Figure 1a demonstrates that anisotropy reduces this value from the isotropic case (1.65) to 1.38, 1.21, and 1.11 for $\langle a_k^2 \rangle = 0.1$, 0.2, and 0.3, respectively. Experimental results range from ~ 0.8 to 1.2.[21, 22, 25]

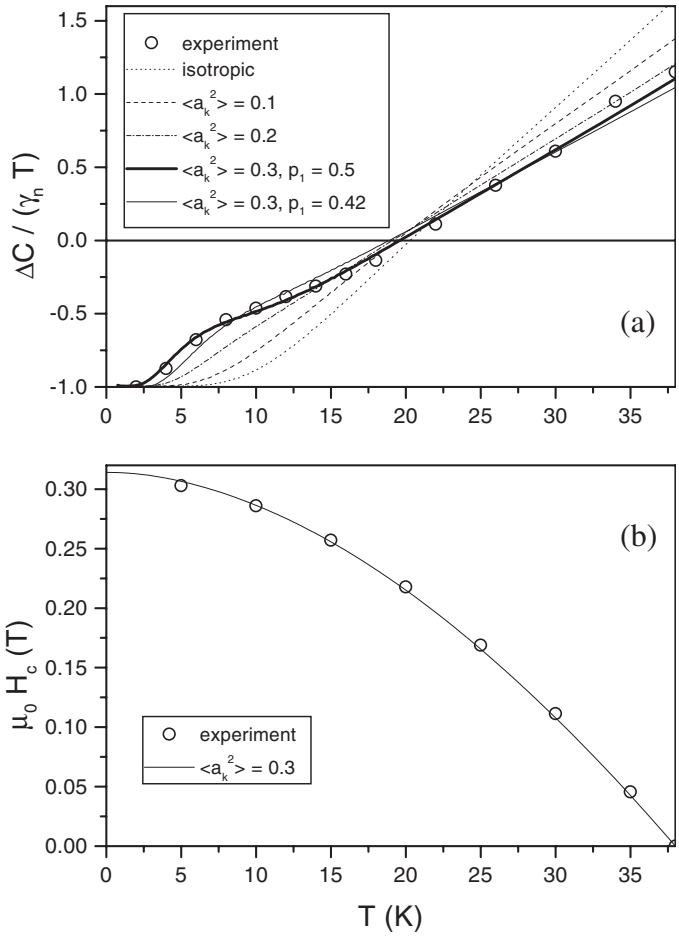

Fig. 1. (a) Specific heat for several anisotropies $\langle a_{\mathbf{k}}^2 \rangle$ compared with experimental data (Ref. 21). The thin solid line shows the effect of changing $p1/p2$ (the relative weights of the density of states) from 1 to 0.42/0.58. (b) Comparison of the calculated thermodynamic critical field ($\langle a_{\mathbf{k}}^2 \rangle = 0.3$, $\gamma_n = 2.68\ \mathrm{mJ\ mol^{-1}\ K^{-2}}$) with measurements on a single crystal.[23]

In the low temperature regime we concentrate on the point, where $\Delta C(T)/(\gamma_n T)$ starts to grow. The onset is determined by the lowest excitation energy of the superconducting state and, therefore, equivalent to the minimum value of the energy gap. As shown in Fig. 1a, this depends again strongly on $\langle a_{\mathbf{k}}^2 \rangle$, because increasing anisotropy leads to weaker coupling and, at the same time, to a smaller gap in one of the sheets (but to an opposite behavior in the other sheet).

With increasing temperature, the slope of $\Delta C(T)/(\gamma_n T)$ changes in the isotropic case smoothly from zero to a positive value, which remains almost constant up to T_c. With anisotropy, we obtain a steeper slope at low or medium temperatures than near T_c, but this becomes significant only for large anisotropies, i.e., for $\langle a_k^2 \rangle > 0.2$ in our model.

We conclude the analysis of the specific heat by comparing our results with measurements reported by Bouquet *et al.*[21] (Fig. 1a, open circles). With an anisotropy parameter $\langle a_k^2 \rangle$ of 0.3 (bold solid line) for MgB_2 excellent agreement with the experimental data is obtained over the whole temperature range in contrast to the other theoretical results shown in Fig. 1a, which are far off especially at low temperatures. We abstain from adjusting $\langle a_k^2 \rangle$ more accurately, because minor differences in the published specific heat curves are obvious, and we are more interested in the qualitative features of the separable model.

Having thus established the value for $\langle a_k^2 \rangle$, we calculate the thermodynamic critical field [Eq. (10)] and fit the data to experimental results on a MgB_2 single crystal[23] by choosing the appropriate γ_n ($H_c \propto \sqrt{\gamma_n}$). The result, shown in Fig. 1b, suggests $\gamma_n = 2.68\ \mathrm{mJ\ mol^{-1}\ K^{-2}}$ which is within the range of published data (~ 2.3–2.8).[21, 22, 25] The isotropic case ($\langle a_k^2 \rangle = \langle b_k^2 \rangle = 0$, $T_c = 38\ \mathrm{K}$) would result in $\gamma_n = 1.92\ \mathrm{mJ\ mol^{-1}\ K^{-2}}$, well outside the experimental margin.

The thermodynamic critical field deviation function $D(T) = [H_c(T)/H_c(0)] - [1 - (T/T_c)^2]$ is negative in the whole temperature range and reaches a minimum of -0.04, slightly below the BCS result. Generally, $D(T)$ grows with coupling strength[24] (and can even become positive), but gets smaller with increasing anisotropy. We find -0.02 for the isotropic case. The fact, that the minimum of the experimentally observed $D(T)$ is -0.02, is not really disturbing, because small absolute errors in the $H_c(T)$ measurement result in large errors in $D(T)$. Furthermore, $H_c(0)$ is not directly accessible from experiment, but has a significant influence on the function, $D(T)$, which increases the uncertainty even more.

3.3. Upper Critical Field

In contrast to $\Delta C(T)$ and $H_c(T)$ the upper critical field $H_{c2}(T)$ is not a thermodynamic property. It depends on the orientation of the applied magnetic field $\mathbf{H}$ due to the anisotropy of the Fermi velocity v_F as a result of an anisotropic Fermi surface. As was pointed out by Prohammer and Schachinger,[15] Eqs. (12)–(15) are only valid for polycrystals, because they contain only averaged information on the anisotropy of the Fermi surface. Nevertheless, the results of these equations can be quite reliable, provided

the average Fermi velocity $\langle v_F \rangle$ and its anisotropy parameter $\langle b_k^2 \rangle$ are used for the relevant plane, i.e., that perpendicular to **H**. To complete the model for $H_{c2}(T)$ we choose opposite signs for $\langle a_k^2 \rangle$ and $\langle b_k^2 \rangle$ [Eq. (16) and (17)] on the same Fermi surface sheet as suggested by de Haas–van Alphen experiments.[26]

The most striking feature of the $H_{c2}^{ab}(T)$ ($\mathbf{H} \parallel ab$) curve (Fig. 2a) is its positive curvature near T_c. It was already demonstrated in Ref. 18, that such a behavior is caused by an anisotropic v_F in the plane perpendicular to **H**. Accordingly, the slope of $H_{c2}(T)$ is constant near T_c for $\langle b_k^2 \rangle = 0$ and the positive curvature emerges and grows with increasing $\langle b_k^2 \rangle$. Good agreement with experiment[6] (open circles in Fig. 2a) is found for $\langle b_k^2 \rangle = 0.4$ ($\langle a_k^2 \rangle = 0.3$) and $\langle v_F \rangle = 7.55 \times 10^5$ m/s, which also reproduces the absolute values ($H_{c2} \propto 1/\langle v_F \rangle^2$) very well. Indeed, band structure calculations[2–4] reveal a strong anisotropy in the corresponding plane and also confirm our mean value of v_F.[27] Similar parameters have been used to successfully describe data on polycrystals, e.g., Ref. 28. We also show, for comparison, the result for an equivalent isotropic system ($\langle a_k^2 \rangle = \langle b_k^2 \rangle = 0$, $T_c = 38$ K, $\mu^* = 0.045$) in Fig. 2a (dotted line). In order to match the low temperature value of $H_{c2}(T)$, $\langle v_F \rangle = 2.51 \times 10^5$ m/s is needed, which is far below the band structure values.[27] If we use, instead, $\langle v_F \rangle = 7.55 \times 10^5$ m/s, we get an extrapolated $\mu_0 H_{c2}(0)$ [$H_{c2}^{iso}(0)$] of only 1.6 T, which is below the experimental value by almost one order of magnitude.

Following these results we also calculate $H_{c2}(T)$ for the applied magnetic field $\mathbf{H} \parallel c$ using the anisotropy parameters $\langle a_k^2 \rangle = 0.3$ and $\langle b_k^2 \rangle = 0.03$, i.e., the mean anisotropy of the Fermi velocity is now much smaller than for $\mathbf{H} \parallel ab$, which is in accordance with theoretical calculations.[2–4] The mean value of the Fermi velocity is $\langle v_F \rangle = 7.50 \times 10^5$ m/s, Ref. 27. The results are shown in Fig. 2a ($\mathbf{H} \parallel c$) and demonstrate excellent agreement with our experimental data (open circles).[6]

In an attempt to investigate the influence of anisotropy on the upper critical field $H_{c2}(T)$ in more detail, we calculate the relative change of $H_{c2}(T)$ with respect to the upper critical field $H_{c2}^{iso}(T)$ of an equivalent isotropic system ($\langle a_k^2 \rangle = \langle b_k^2 \rangle = 0$) having the same $T_c = 38$ K and the same average e^--ph coupling and Fermi velocity as the anisotropic system. Thus, the ratio $H_{c2}(T)/H_{c2}^{iso}(T)$ will only depend on the two anisotropy parameters. Figures 2b, c show the results for this ratio in two cases, namely, as a function of $\langle b_k^2 \rangle$ for a fixed value $\langle a_k^2 \rangle = 0.3$ and as a function of $\langle a_k^2 \rangle$ for a fixed value of $\langle b_k^2 \rangle = 0.4$ with μ^* adjusted to keep T_c constant. Concentrating on Fig. 2b, we see that $H_{c2}(T)$ of an anisotropic system with $\langle a_k^2 \rangle \neq 0$ and $\langle b_k^2 \rangle = 0$ is shifted to higher values, almost constantly for all temperatures and without showing an upward curvature close to T_c. In

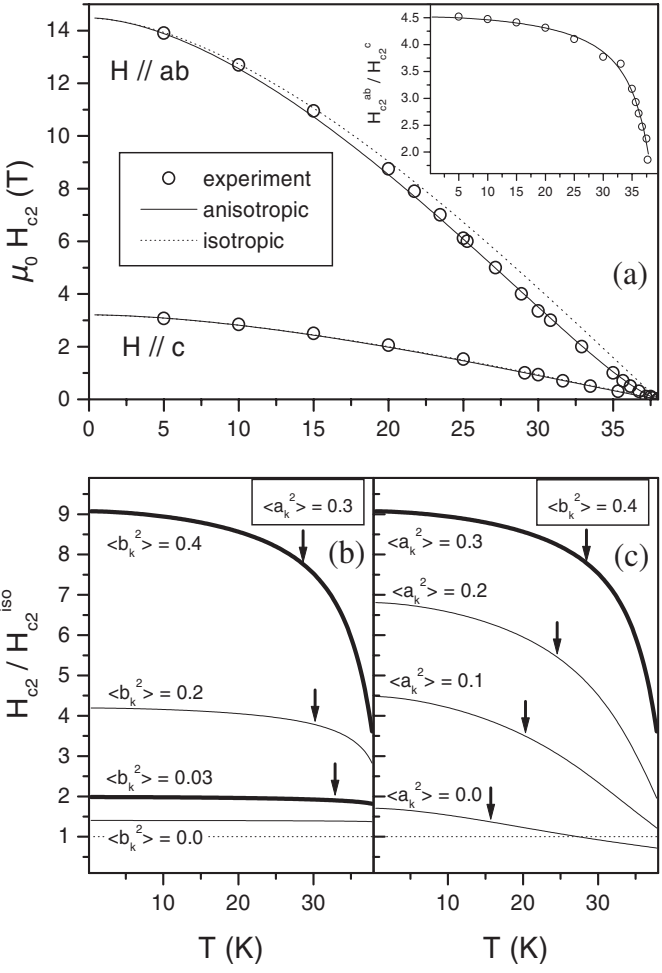

Fig. 2. (a) Upper critical field of MgB_2. The solid lines represent the best anisotropic fit for $H \| ab$ ($\langle a_k^2 \rangle = 0.3$, $\langle b_k^2 \rangle = 0.4$, and $\langle v_F \rangle = 7.55 \times 10^5$ m/s) and $H \| c$ ($\langle a_k^2 \rangle = 0.3$, $\langle b_k^2 \rangle = 0.03$, and $\langle v_F \rangle = 7.50 \times 10^5$ m/s), the dotted lines isotropic fits ($\langle a_k^2 \rangle = \langle b_k^2 \rangle = 0$, with $\langle v_F \rangle = 2.51 \times 10^5$ m/s for $H \| ab$ and $\langle v_F \rangle = 5.31 \times 10^5$ m/s for $H \| c$) to the experimental data (open circles).[23] Inset: Upper critical field anisotropy H_{c2}^{ab}/H_{c2}^{c}. (b) and (c) Relative deviation of the anisotropic $H_{c2}(T)$ from the isotropic behavior $H_{c2}^{iso}(T)$ at fixed $\langle v_F \rangle$. The bold solid lines correspond to the best fits shown in panel (a), i.e., $\langle a_k^2 \rangle = 0.3$, $\langle b_k^2 \rangle = 0.4$ for $H \| ab$ and $\langle a_k^2 \rangle = 0.3$, $\langle b_k^2 \rangle = 0.03$ for $H \| c$. (b) Effect of varying the v_F anisotropy $\langle b_k^2 \rangle$ at fixed coupling anisotropy $\langle a_k^2 \rangle = 0.3$, and (c) effect of varying $\langle a_k^2 \rangle$ at fixed $\langle b_k^2 \rangle = 0.4$. The arrows indicate the temperature, where the curvature of H_{c2} switches from negative to positive values.

contrast, $H_{c2}(T)$ for $\langle a_{\mathbf{k}}^2 \rangle = 0$ (Fig. 2c) increases with $\langle b_{\mathbf{k}}^2 \rangle$ only at low temperatures, but even decreases near T_c and develops a significant upward curvature.

The results presented in Figs. 2b, c reveal nicely the competing influence of the two anisotropy parameters on the temperature dependence of $H_{c2}(T)$. Keeping $\langle a_{\mathbf{k}}^2 \rangle$ constant and increasing $\langle b_{\mathbf{k}}^2 \rangle$ shifts the turning point in the $H_{c2}(T)$ curve towards lower temperatures (as indicated by the down arrows in Fig. 2b) thus making the upward curvature of $H_{c2}(T)$ close to T_c more pronounced and the (relative) slope of $H_{c2}(T)$ at T_c flatter (with respect to $H_{c2}(0)$). On the other hand, keeping $\langle b_{\mathbf{k}}^2 \rangle > 0$ constant and increasing $\langle a_{\mathbf{k}}^2 \rangle$ results in just the opposite behavior, as indicated in Fig. 2c, namely the turning point in the $H_{c2}(T)$ curve is moved towards higher temperatures and the (relative) slope of $H_{c2}(T)$ at T_c remains nearly unaffected (and brings the relative curves closer to the isotropic behavior). The results presented in Figs. 2b, c prove that appropriate combinations of the two anisotropy parameters can result in an increase of the zero temperature upper critical field $H_{c2}(0)$ over its isotropic equivalent by almost one order of magnitude, while "turning on" just one of the two parameters has rather little effect.

Finally, the inset of Fig. 2a shows the calculated anisotropy of H_{c2}, $\gamma = H_{c2}^{ab}/H_{c2}^{c}$, which nicely reproduces the pronounced temperature dependence of the experimental data.[5–7] Similar curves were obtained recently by Dahm and Schopol,[29] who employed a more realistic Fermi surface for MgB_2. In their calculations based on the Eilenberger formalism, $\gamma(T)$ depends on the Fermi surface anisotropy (of the σ-band) and on the interband coupling of the two bands. In our model, $\gamma(T)$ directly reflects the specific properties of H_{c2}^{ab}, i.e., being mainly determined by the (mean) anisotropy of the Fermi velocity, which should, therefore, be a rather common feature for strongly anisotropic superconductors (exhibiting s-wave pairing and e^--ph coupling). The effect of varying $\langle a_{\mathbf{k}}^2 \rangle$ or $\langle b_{\mathbf{k}}^2 \rangle$ (in the plane perpendicular to *ab*) is similar to that of $H_{c2}/H_{c2}^{\mathrm{iso}}$ in Figs. 2b and c (but with different absolute values), since the temperature dependence of H_{c2}^{c} differs only slightly from the isotropic case.

3.4. Physical Relevance

We now turn to a short discussion of the physical relevance of our calculations and the resulting parameters. In principle, the separable model is designed for small anisotropies in the e^--ph coupling of superconductors, which is certainly not fulfilled for $\langle a_{\mathbf{k}}^2 \rangle = 0.3$. To check for possible errors, we note, that the anisotropic coupling $\lambda_{\mathbf{k},\mathbf{k}'}$ and other functions can be described by a series of Fermi surface harmonics.[30] If we stop the

expansion after the first term, i.e., use Fermi surface harmonics only of zeroth order, we get the separable model.[18] Thus, it is quite plausible that the most significant features of the system can be described by this simplified model, which is useful for the understanding of specific anisotropy effects caused by e^--ph coupling and Fermi velocity anisotropy in MgB_2, whereas they are difficult to explain using the fully anisotropic theory. Errors made by ignoring higher order terms, can partly be balanced by the anisotropy parameters. Thus, if we adjust these parameters to reveal the correct macroscopic effects, we cannot expect to get the correct microscopic quantities as well. Nevertheless, we will show in the following, that the deviations are not too large.

To get a second perspective on our approximations, we can interpret the separable model as a special case of the (isotropic) two band model.[31] The appropriate coupling strengths are $\lambda_{11} = 0.73$, $\lambda_{22} = 0.06$, $\lambda_{12} = \lambda_{21} = 0.21$, determined from $\lambda_{ij} = p_j(1+a_{si})\,\lambda(1+a_{sj})$ (note that $\langle\lambda_{\mathbf{k},\mathbf{k}'}\rangle' = p_1\lambda_{\mathbf{k},s1} + p_2\lambda_{\mathbf{k},s2}$ in our separable model). A wide range of λ values was found in ab-initio calculations[9, 10, 19, 20] as well as in de Haas–van Alphen experiments,[26] with λ clustering at small and large values, respectively. In some cases, averaged $\lambda_{\mathbf{k},\mathbf{k}'}$ distributions were used and applied to the isotropic two band model.[9, 32, 33] Our λ_{11} (0.73) and the interband coupling λ_{12} (0.21) are comparable with such averages, but λ_{22} (0.06) is significantly smaller. In particular, we find $\lambda_{22} < \lambda_{12}, \lambda_{21}$, in contrast to other results. To test the influence of such different parameters, we solve the Eb equations for $\lambda_{11} = 1.017$, $\lambda_{22} = 0.448$, $\lambda_{12} = 0.213$, and $\lambda_{21} = 0.155$ (cf. Ref. 32), but this model does not reproduce the pronounced bump in the specific heat curve at low temperatures very well. Only when λ_{22} is decreased, the experimental behavior is approached. Furthermore, we calculate the energy gaps on the two bands and find $\Delta_1 = 6.4$ meV, $\Delta_2 = 1.7$ meV at 0 K, in reasonable agreement with experiment.[34–37]

The parameters $\langle a_{\mathbf{k}}^2\rangle$ and $\langle b_{\mathbf{k}}^2\rangle$ also have to compensate for other simplifications mentioned at the beginning of this section. We assume, e.g., equal electronic density of states in both bands ($p_1 = p_2 = 0.5$), but band structure calculations show $p_1 = 0.42$–0.45 and $p_2 = 0.58$–0.55.[9, 10, 19, 20] However, our model calculations with such weights and slightly modified parameters lead to similar results (the thin solid line in Fig. 1a, e.g., shows the effect of changing p_1/p_2 to 0.42/0.58, which is in less good agreement with the data, but can be compensated by a slight increase of $\langle a_{\mathbf{k}}^2\rangle$ to 0.33). Furthermore, we find, that increasing the width of the peak in the Eb function from 1 meV to 10 meV, has almost no effect on the temperature dependence of our main results. Impurities were not considered, because we suppose the samples, used for the data analysis in this paper, to be in the clean limit, which in particular holds for the dominant σ band.

4. CONCLUSIONS

We presented a detailed analysis of anisotropy effects in MgB_2 solving the Eliashberg equations for a separable model anisotropy together with an e^--ph interaction spectral density $\alpha^2F(\omega)$ described by an Einstein spectrum with the peak centered around 76 meV. We demonstrated that the separable model, although very simple, is capable of reproducing experimental data for the thermodynamics and for the upper critical field $H_{c2}(T)$ in high quality MgB_2 single crystals in the direction $\mathbf{H} \parallel ab$-plane as well as $\mathbf{H} \parallel c$-axis. This analysis allows to describe the mean square anisotropy of the e^--ph coupling ($\langle a_{\mathbf{k}}^2 \rangle$) and of the Fermi velocity ($\langle b_{\mathbf{k}}^2 \rangle$) within the *ab*-plane and along the *c*-axis. Using only these two parameters, we obtain the "unconventional" properties of MgB_2 and due to the very simple and concrete physical interpretation of these two parameters in our model, we find a simple and clear picture of the particular reasons responsible for a particular effect. E.g., the kink in the specific heat curve emerges and becomes more pronounced with increasing $\langle a_{\mathbf{k}}^2 \rangle$. The positive curvature in $H_{c2}^{ab}(T)$ depends in the same way on $\langle b_{\mathbf{k}}^2 \rangle$ but is reduced by an increasing $\langle a_{\mathbf{k}}^2 \rangle$. The simplicity of the model also suggests, that many of the unusual effects in MgB_2 are very general for strongly anisotropic superconductors (with e^--ph coupling and s-wave pairing) and do not strongly rely on the particular shape and properties of the Fermi surface, but rather on the mean values and mean anisotropies. It should be noted, that the separable model can be interpreted as a two band, but also as an anisotropic single band model, i.e., the properties of MgB_2, addressed in this article, cannot be regarded as a proof of two band superconductivity in any material (this holds in particular for obtaining a kink in measurements of the specific heat). Our results show, moreover, that the coupling of the electrons to this single 76 meV phonon mode is, together with strong anisotropy, the dominant feature responsible for the superconducting properties of MgB_2. This result is in full agreement with the study by Golubov *et al.*[32] and by Dolgov *et al.*,[38] who showed that, within a two-band model, basically $\alpha^2F_{\sigma\sigma}(\omega)$ dominates, which has a very prominent peak at ~ 76 meV accompanied by much smaller structures at lower energies. The interband spectral density $\alpha^2F_{\sigma\pi}(\omega)$ also shows this peak, but not as pronounced, and thus gives only a minor contribution to the $\alpha^2F(\omega)$ responsible for the *ab*-plane properties of MgB_2.

ACKNOWLEDGMENTS

This work was supported in part by the Austrian Science Foundation under Grant No. 14222.

REFERENCES

1. For a review, see *Physica C* **385**, (2003).
2. J. Kortus, I. I. Mazin, K. D. Belashchenko, V. P. Antropov, and L. L. Boyer, *Phys. Rev. Lett.* **86**, 4656 (2001).
3. S. V. Shulga, S.-L. Drechsler, H. Eschrig, H. Rosner, and W. E. Pickett, cond-mat/0103154 (unpublished).
4. K. D. Belashchenko, M. van Schilfgaarde, and V. P. Antropov, *Phys. Rev. B* **64**, 092503 (2001).
5. M. Angst, R. Puzniak, A. Wisniewski, J. Jun, S. M. Kazakov, J. Karpinski, J. Roos, and H. Keller, *Phys. Rev. Lett.* **88**, 167004 (2002).
6. M. Zehetmayer, M. Eisterer, H. W. Weber, J. Jun, S. M. Kazakov, J. Karpinski, and A. Wisniewski, *Phys. Rev. B* **66**, 052505 (2002).
7. L. Lyard, P. Samuely, P. Szabo, T. Klein, C. Marcenat, L. Paulius, K. H. P. Kim, C. U. Jung, H.-S. Lee, B. Kang, S. Choi, S.-I. Lee, J. Marcus, S. Blanchard, A. G. M. Jansen, U. Welp, G. Karapetrov, and W. K. Kwok, *Phys. Rev. B* **66**, 180502 (2002).
8. S. Manalo and E. Schachinger, *J. Low Temp. Phys.* **123**, 149 (2001).
9. A. Y. Liu, I. I. Mazin, and J. Kortus, *Phys. Rev. Lett.* **87**, 087005 (2001).
10. H. J. Choi, D. Roundy, H. Sun, M. L. Cohen, and S. G. Louie, *Phys. Rev. B* **66**, 020513 (2002).
11. I. I. Mazin, O. K. Andersen, O. Jepsen, A. A. Golubov, O. V. Dolgov, and J. Kortus, cond-mat/0212417 (unpublished).
12. V. G. Kogan, *Phys. Rev. B* **66**, 020509 (2002).
13. D. Markowitz and L. P. Kadanoff, *Phys. Rev.* **131**, 563 (1963).
14. M. Daams and J. P. Carbotte, *J. Low Temp. Phys.* **43**, 263 (1981).
15. M. Prohammer and E. Schachinger, *Phys. Rev. B* **36**, 8353 (1987).
16. P. B. Allen and B. Mitrovic, in *Solid State Physics*, H. Ehrenreich, F. Seitz, and D. Turnbull (eds.), Academic, New York (1982).
17. J. Bardeen and M. Stephen, *Phys. Rev.* **136**, A1485 (1964).
18. W. Pitscheneder and E. Schachinger, *Phys. Rev. B* **47**, 3300 (1992).
19. Y. Kong, O. V. Dolgov, O. Jepsen, and O. K. Andersen, *Phys. Rev. B* **64**, 020501 (2001).
20. K.-P. Bohnen, R. Heid, and B. Renker, *Phys. Rev. Lett.* **86**, 5771 (2001).
21. F. Bouquet, R. A. Fisher, N. E. Phillips, D. G. Hinks, and J. D. Jorgensen, *Phys. Rev. Lett.* **87**, 047001 (2001).
22. Y. Wang, T. Plackowski, and A. Junod, *Physica C* **355**, 179 (2001).
23. Experimental details are described in Ref. 6, but may differ slightly due to sample-to-sample variations.
24. J. P. Carbotte, *Rev. Mod. Phys.* **62**, 1027 (1990).
25. H. D. Yang, J.-Y. Lin, H. H. Li, F. H. Hsu, C. J. Liu, S.-C. Li, R.-C. Yu, and C.-Q. Jin, *Phys. Rev. Lett.* **87**, 167003 (2001).
26. E. A. Yelland, J. R. Cooper, A. Carrington, N. E. Hussey, P. J. Meeson, S. Lee, A. Yamamoto, and S. Tajima, *Phys. Rev. Lett.* **88**, 217002 (2002).
27. Reference 4 states for the components of v_F: $\langle v_{F,x}\rangle \cong \langle v_{F,y}\rangle = 5.36\times10^5$ m/s and $\langle v_{F,z}\rangle = 4.85\times10^5$. We find $\langle v_F\rangle = \sqrt{\langle v_{F,x}\rangle^2+\langle v_{F,z}\rangle^2} = 7.23\times10^5$ m/s for H_{c2}^{ab} and $\langle v_F\rangle = \sqrt{\langle v_{F,x}\rangle^2+\langle v_{F,y}\rangle^2} = 7.58\times10^5$ m/s for H_{c2}^{c}.
28. S. L. Bud'ko and P. C. Canfield, *Phys. Rev. B* **65**, 212501 (2002).
29. T. Dahm and N. Schopohl, *Phys. Rev. Lett.* **91**, 17001 (2003).
30. P. B. Allen, *Phys. Rev. B* **13**, 1416 (1976).
31. H. Suhl, B. T. Matthias and L. R. Walker, *Phys. Rev. Lett.* **3**, 552 (1959).
32. A. A. Golubov, J. Kortus, O. V. Dolgov, O. Jepsen, Y. Kong, O. K. Andersen, B. J. Gibson, K. Ahn, and R. K. Kremer, *J. Phys. Condens. Mat.* **14**, 1353 (2002).
33. I. I. Mazin and V. P. Antropov, *Physica C* **385**, 49 (2003).
34. P. Szabó, P. Samuely, J. Kamarík, T. Klein, J. Marcus, D. Fruchart, S. Miraglia, C. Marcenat, and A. G. M. Jansen, *Phys. Rev. Lett.* **87**, 137005 (2001).

35. H. Schmidt, J. F. Zasadzinski, K. E. Gray, and D. G. Hinks, *Phys. Rev. Lett.* **88**, 127002 (2002).
36. M. Iavarone, G. Karapetrov, A. E. Koshelev, W. K. Kwok, G. W. Crabtree, D. G. Hinks, W. N. Kang, E.-M. Choi, H. J. Kim, H.-J. Kim, and S. I. Lee, *Phys. Rev. Lett.* **89**, 187002 (2002).
37. R. S. Gonnelli, D. Daghero, G. A. Ummarino, V. A. Stepanov, J. Jun, S. M. Kazakov, and J. Karpinski, *Phys. Rev. Lett.* **89**, 247004 (2002).
38. O. V. Dolgov, R. S. Gonnelli, G. A. Ummarino, A. A. Golubov, S. V. Shulga, and J. Kortus, cond-mat/0301542 (unpublished).